Self-Attenuating Real-Time Vibration Control of a Flexible Long-Reach Robot

Anthony Siming Chen[1,2,†], Erwin Jose Lopez Pulgarin[2], Guido Herrmann[2], Alexander Lanzon[2], Joaquin Carrasco[2], Barry Lennox[2], John Brotherhood[3], Tomoki Sakaue[4], and Kaiqiang Zhang[5]

***Abstract*—We address the critical challenge of vibration control of flexible long-reach robot manipulators used in nuclear decommissioning. The research is motivated by the urgent need to ensure precision and safety during the deployment of robotic systems in confined and hazardous environments, such as the through-wall deployment (TWD) system for the Sellafield nuclear site. The TWD system, featuring a rigid manipulator on a flexible two-link boom, is designed to maneuver through small openings in containment vessels. While this design avoids the need for bulky structures, the slenderness of the boom makes it prone to significant vibrations, potentially compromising the system's stability and accuracy. To address these challenges, we propose a novel real-time flexible control system that suppresses vibrations using only the robot manipulator's own actuation, without requiring additional actuators. The control strategy is based on the mixed-sensitivity H_∞ synthesis for a dedicated dynamics model via inertial sensing, enhancing the robustness and adaptability over the multi-modal flexibilities. Experimental validation demonstrated the control system's effectiveness in reducing vibrations, thereby improving operational efficiency and safety. These findings have broader implications for deploying flexible, intelligent control systems in other high-stakes environments, such as the Fukushima Daiichi site, where similar vibration-related challenges are encountered.**

***Index Terms*—Long-reach robot, flexible robot, vibration control, H_∞ synthesis, robot manipulator, nuclear robotics**

I. Introduction

THE increasing dependence on robotics is transforming the landscape of remote maintenance, particularly in scenarios where direct human intervention is impractical or hazardous. These robots are often tasked with operating in unconventional and hard-to-access areas, such as being mounted on extended booms, deployed inside high-rise structures, or functioning in environments subject to constant vibration and movement. Their deployment in these settings is not just a matter of convenience but a critical factor in maintaining operational continuity and safety. By performing maintenance in such challenging conditions, these robots help to minimize downtime, prevent potential hazards, and ensure that essential systems and infrastructure continue to function optimally. This technological advancement allows for continuous monitoring and repair work in environments that would otherwise be too risky or inaccessible for human workers, thereby revolutionizing the maintenance process across various industries.

Fig. 1: A picture of the 3-D CAD model of the TWD system.

A. Unique Challenge — Manipulator on a Flexible Base

This work is motivated by the urgent need for effective vibration control in flexible long-reach robotic manipulators used in nuclear decommissioning. Specifically, it addresses the *through-wall deployment* (TWD) system, which features a rigid robot manipulator mounted on the end of a flexible long-reach two-link boom. Fig. 1 displays a 3-D *computer-aided design* (CAD) model of the system. This TWD system was recently conceptualized and fabricated by Amentum (formerly Jacobs) for decommissioning. It was designed to be deployed through a small hole in the wall of a containment vessel/cell at, e.g., the Sellafield nuclear site in the United Kingdom. To meet stringent spatial constraints on-site, the flexible long boom manipulator design avoids the need for massive and bulky structures. However, its slenderness is prone to significant unwanted vibrations. Likewise, the long-reach system prototyped at the Fukushima Daiichi Nuclear Power Plant in Japan encounters similar issues with vibrations [1]. Therefore,

This work was funded by the UK Atomic Energy Authority (UKAEA) within the scope of the LongOps program. The work was partially funded by the UKRI Advanced Machinery Productivity Institute (AMPI), and supported by UKAEA/EPSRC Fusion Grant 2022/27 (EP/W006839/1) for fusion decommissioning, by the RAICo Fellowship, and by the University of Nottingham through Faculty of Engineering Early Career Award. Any opinions, findings, and conclusions or recommendations expressed in this material are those of the authors and do not necessarily reflect the views of the sponsors. (†*Corresponding author: Anthony Siming Chen. Email:* a.chen@nottingham.ac.uk, siming.chen@manchester.ac.uk)

[1]A.S. Chen is with the Mechanical and Aerospace Research Group (MAS), Department of Electrical and Electronic Engineering, University of Nottingham, NG7 2RD Nottingham, United Kingdom.

[2]A.S. Chen, E.J. Lopez Pulgarin, G. Herrmann, A. Lanzon, J. Carrasco, and B. Lennox are with the Control Systems and Robotics Group (CSR), Department of Electrical and Electronic Engineering, The University of Manchester, M13 9PL Manchester, United Kingdom.

[3]J. Brotherhood is with Amentum (formerly Jacobs), 601 Faraday Street, Birchwood, Warrington, WA3 6GN, United Kingdom.

[4]T. Sakaue is with Tokyo Electric Power Company (TEPCO) Holdings, Fukushima, Japan.

[5]K. Zhang is with the United Kingdom Atomic Energy Authority (UKAEA), Culham Campus, OX14 3DB, United Kingdom.

the goal of this work is to develop a real-time feedback control system that is capable of actively mitigating the vibrations from the flexible long-reach boom by optimally actuating the robot manipulator.

Most existing control and path planning methods [2] for robot manipulators focus on grasping/handling objects or avoiding obstacles, where the base of a manipulator is usually assumed to be fixed at a rigid base [3]. The trajectories within either the joint space or the task space are designed concerning general features such as initial/final point, duration, maximum velocity, etc., while the vibration it generates to the environment or the vibration of the manipulator itself is neglected. This is true for common use cases where the base of a manipulator is stationary, e.g., it is mounted to the ground or a heavy-duty workstation. When the base of a manipulator is flexible, e.g., the manipulator is mounted on a flexible long-reach boom or a mobile platform, the vibration becomes no longer negligible. The motion of any manipulator's joints or end effector generates an overall force/torque at the manipulator's base. Such force/torque applied to the flexible base, if not specifically minimized, can result in significant undesired vibration. The vibration at the base easily translates to the vibration at the end effector, which could be detrimental to the tasks. In the case of performing laser cutting at the end effector, even a small amount of vibration can produce large unwanted cuts.

B. Related Work

There exist earlier studies of manipulators with flexible bases such as *mobile manipulators* [4]–[7], but their vibration was never considered. Particularly, Tahboub [7] designed an observer-based controller for a manipulator with a moving base, but it focused on rejecting only a single unwanted disturbance force from the base instead of multi-modal vibrations. There is generally a limited understanding of how the motion of a manipulator's joints and end-effector induces vibration at its base, especially when the base itself is flexible. It is important to distinguish that our TWD system combines a rigid industrial manipulator with a flexible long-reach boom, which differs from common notion of *flexible manipulators* [8]–[12] or *soft manipulators* [13], [14], where the flexibility lies within the manipulator itself (in one or more links or joints). Consequently, most vibration control methods developed for flexible manipulators, such as those mentioned in the comprehensive surveys [15], [16], cannot be directly applied to this TWD system. However, the underlying methodology might still be relevant for addressing flexibility issues in this context. Among the literature, robust control methods [17], [18] have consistently been popular for addressing flexibility, as they are effective in handling uncertainties and disturbances, such as sliding-mode control in [17] and switching control in [18]. On the other hand, intelligent control methods [19]–[23], using neural networks and learning-based approaches, have also gained traction for tackling flexibility issues due to their ability to adapt to complex dynamics and varying conditions. However, many of these studies employed simplified models of flexible manipulators or were model-free, often reducing the system to a single-link structure, e.g., [21]–[23]. This simplification was necessary because learning-based controllers typically require a manageable and less complex model to effectively train and validate their algorithms, which helps reduce computational complexity and improve the efficiency of the learning process. However, the whole TWD system (manipulator + boom) is essentially a multi-link structure which introduces significantly more complexity and dynamic interactions. The studies in [24] and [25] addressed "rigid-flexible" systems structurally similar to ours. The actuation is a single joint between the links in [24], which differs from the TWD with no actuation between the manipulator and the boom. In [25], the rigid manipulator was simplified to three identical links and the results lack experimental validation. Both studies were limited to open-loop trajectory planning without closed-loop vibration damping.

There are studies specifically considering the disturbance from the manipulator base, including space manipulators [26]–[29], as well as underwater [30] and aerial manipulators [31]. Qiao *et al.* [26] proposed a nonlinear disturbance observer-based control scheme to achieve high-precision attitude tracking for space manipulators under multiple disturbances. The computational complexity of implementing nonlinear disturbance observers in real-time could pose challenges for systems with limited processing capabilities. [31] addressed translational disturbance rejection for jet-actuated flying continuum robots operating on mobile bases. They designed an H_∞-based controller to suppress vibrations and enhance stability during rapid maneuvers, which is crucial for aerial robots performing tasks in dynamic and unstructured environments.

There is a limited number of control design approaches suited for the use case in this paper, i.e., it requires a systematic and efficient use of complex plant dynamics in a closed-loop design to achieve a flexible controller for the effective real-time compensation of possible exogenous effects, such as disturbances. In linear systems' theory, possible approaches are model-based approaches such as optimal control [32], H_2 control [32], *model predictive control* (MPC) [33], and ultimately H_∞ control [34]. Here, optimal and H_2 control do not easily allow for dynamic uncertainty and disturbances, while the MPC is generally directed to slower dynamics or very fast, highly powered control implementation hardware. The H_∞ control approach is useful as it allows to include an explicit understanding of system uncertainty and actuator limitations in addition to multiple performance requirements. Thus, frequency shaping through a mixed-sensitivity approach toward control design is highly desirable and not easily achievable with other control approaches such as optimal control or MPC. Alternatively, other control approaches preferably require matching of actuation and sources of uncertainty and disturbances, e.g. sliding-mode control (SMC, e.g. [17]) or Active Disturbance Rejection Control (ADRC, [35]); in case of high order systems and multiple control objectives, the design of ADRC and SMC has to be observer-based. ADRC will have to involve multiple cascaded loops to satisfy the matching condition [35]. In contrast, the limitation is that the tools of H_∞ control have been developed for plant systems with mild nonlinearities, which is sufficiently satisfied for manipulator

motion.

C. Contributions

Building upon the above studies, this paper addresses the unique challenge of vibration suppression of the TWD system within nuclear environments by introducing a real-time active flexible control strategy. Instead of relying on low-bandwidth control and slow manipulator movements, our approach emphasizes a deep understanding of the dynamic *interaction* between the rigid manipulator and its flexible base (boom). This is different from most studies on flexible manipulators that focused on their *internal* flexibility instead of their *interaction* with the environments. This insight enables precise and fast control of the manipulator to prevent boom excitation, allowing for rapid and efficient manipulator operation.

We summarize the key contributions:

1) *Vibration Control via Manipulator Actuation Only*: This work enables boom vibration suppression using only the manipulator's own actuation, without any additional actuators. Through frequency-domain identification of multi-modal resonance behavior and embedding uncertainty directly into the control synthesis, this approach is well suited to practical deployment in flexible-base industrial robots.

2) *Discrete Joint Velocity-Based Feedback Implementation*: We implement a practical discrete-time H_∞ controller that enables vibration suppression using only joint velocity actuation, without access to torque-level control. This addresses several real-world challenges: (i) velocity-only actuation interfaces on commercial manipulators, (ii) integration of inertial sensing feedback from the flexible boom, (iii) real-time closed-loop implementation at 500 Hz, and (iv) robustness against unmodeled nonlinear coupling between the manipulator and boom. The controller is synthesized based on experimentally identified dynamics, ensuring compatibility with industrial hardware and reliability in complex environments.

3) *Comprehensive Design and Experimental Validation*: The approach is validated both in simulation and experimentally on the real TWD system, achieving an average vibration reduction of 80% across multiple configurations. We present a structured workflow encompassing frequency-domain system identification, discrete-time controller synthesis, and real-time implementation. Designed with the hardware and software constraints of commercial manipulators in mind, our method offers a transferable solution for similar industrial systems.

The rest of the paper is structured as follows. Section II introduces the TWD system and its dynamic modeling. Section III presents the flexible control design. Section IV provides the real-time implementation via a design modification for joint velocity actuation rather than joint position. Section V demonstrates the simulation/experiment results and their implications. Section VI concludes the paper with further research opportunities.

II. TWD System and Its Dynamics Modeling

This section provides a basic description of the TWD system and the modeling process of its dynamics.

A. The TWD System

The TWD system developed by Amentum is a flexible long-reach robotic manipulator system used to address the challenges in nuclear decommissioning. The TWD system consists of a rigid robotic manipulator: Doosan Robotics Cobot M1013 (1.3 m reach), mounted at the end of a flexible long-reach two-link boom (mild steel), where the boom is made of a 5 m main boom (the first link) hinged with a 1 m rotating boom (the second link), as shown in Fig. 1. The system is designed to be deployed through a small hole in the wall which supports nuclear decommissioning where the robotic manipulator can provide a) sensor positioning to characterize the target and b) tooling, for instance, laser cutting.

TABLE I: Specifications of the robot manipulator.

Manipulator model	Doosan Robotics Cobot M1013
Weight	33kg
Payload	10kg
Maximum operating radius	1300mm
Number of axes	6
Operation angle and Maximum speed of each axis	Joint 1 ±360° 120°/s Joint 2 ±360° 120°/s Joint 3 ±160° 180°/s Joint 4 ±360° 225°/s Joint 5 ±360° 225°/s Joint 6 ±360° 225°/s

Given that the TWD system consists of two parts: 1) a flexible long-reach boom and 2) a rigid robotic manipulator, it is reasonable to model the system dynamics for each part. Modeling of the Doosan Robotics Cobot manipulator is relatively straightforward as it is a commercial product. Table I provides the basic specifications of the M1013 model. A numerical model of the manipulator can be generated using the off-the-shelf CAD design [36] along with the given physical parameters, i.e. kinematics information, masses and inertias. Here we focus on explaining the modeling process for the flexible long-reach boom dynamics.

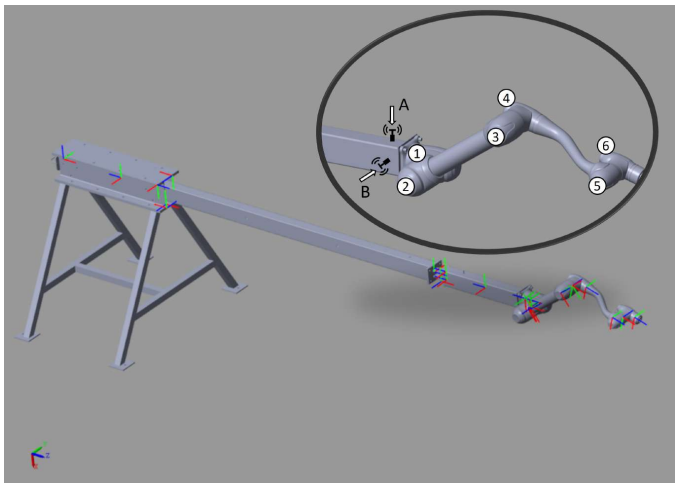

Fig. 2: TWD system simulation model in Matlab/Simscape.

To begin with, under a normal working condition, the vibration of the system is induced by the motion of the Doosan Robotics Cobot manipulator. The vibration at the end

effector is crucial, e.g., when executing laser cutting at the end effector, even the slightest vibration can be disastrous. The motion of any manipulator's joints or end effector generates an overall force/torque at the manipulator's base. Assuming the manipulator is a rigid body, the vibration of the end effector is directly translated from the vibration at the end of the boom since the manipulator base is mounted there. Therefore, we focus on understanding the modal characteristics of the boom, i.e., how the force or torque generated from the manipulator translates to the vibration of the boom's end. This also provides a better understanding of the robotic manipulator in relation to the environment.

B. Data Collection

The vibration tests were performed using a PCB 086C03 impact hammer and a pair of PCB 353B33 accelerometers. Fig. 2 presents a diagram of the TWD system simulation model showing the sensor installation (an accelerometer at point A measuring the vertical acceleration and an accelerometer at point B measuring horizontal acceleration). These two measurements are important for assessing the overall vibration of the TWD system because these measurement points A and B reflect the vertical (X axis) and horizontal (Y axis) acceleration of the end of the boom, respectively. In principle, the impact tests were carried out covering a wide range of the operating conditions of the flexible long-reach boom, which includes 4 configurations while the robotic manipulator remains fixed and non-actuated (see Fig. 3). The four boom configurations were selected to evaluate the controller's robustness across varying resonance frequencies and dynamic behaviors due to differences in boom length and hinge angles. The full-length boom with a 180-degree hinge angle (Configuration 1) exhibits the lowest natural frequencies and highest flexibility, making it more prone to large deflections and resonance effects. Reducing the hinge angle to 90 degrees (Configuration 2) increases structural stiffness, shifting resonance frequencies higher while still allowing moderate flexibility. A further reduction to 45 degrees (Configuration 3) results in a compromise between flexibility and rigidity, altering modal frequencies accordingly. Finally, the half-length boom with a 180-degree hinge angle (Configuration 4) significantly increases stiffness, leading to higher resonance frequencies and lower vibration amplitudes. These variations were designed to systematically assess how changes in boom geometry influence the system's dynamic behavior and to ensure that the control approach remains effective across different structural conditions. A National Instruments (NI) data acquisition device USB-4431 enables real-time dynamic data collection. Both points A and B were closely hit with the impact hammer and recorded for 30 seconds at a sampling frequency of 1000 Hz. We carried out an experimental modal analysis which provides a set of frequency response functions (FRFs) that contain information about resonance frequencies, damping, and mode shape. For example, under Configuration 1, it is obtained that the first three modal frequencies for point A are 3.8 Hz, 14.1 Hz, and 29.8 Hz. The FRF (i.e. the ratio of the Fourier Transform of the acceleration measurement divided by the Fourier Transform of the force excitation) is particularly important for the development of an input-output transfer function model.

Fig. 3: Photos of the 4 boom configurations (Configuration 1: Full-length boom with 180-degree hinge angle; Configuration 2: Full-length boom with 90-degree hinge angle; Configuration 3: Full-length boom with 45-degree hinge angle; Configuration 4: Half-length boom with 180-degree hinge angle).

C. Dynamics Modeling

The purpose of the boom model is to provide realistic vibration responses given the input forces. The model should capture the computed FRF characteristics and be able to reproduce a fairly accurate vibration measurement. Therefore, the boom model is created as a set of transfer functions fitted from the FRFs to characterize the realistic vibration dynamics. It outputs the vibration response, i.e. acceleration, velocity, and position at the pre-selected points A and B. The FRFs characterize how the system responds to excitations at different frequencies, encapsulating both the amplitude and phase relationships between input forces and output responses [37].

Based on the collected and processed data, a TWD simulation model is created in Matlab/Simscape. The model integrates two parts: the boom model and the robotic manipulator model. The manipulator model is created using Simscape Multibody Toolbox, which enables control via either motion or torque at each joint out of the total six joints. By adding a virtual joint at the base (the connecting face) of the manipulator between the manipulator and the boom, the model outputs the composite forces $\boldsymbol{f}$ in X, Y, and Z axis directions. We have used position feedback to move the X-Y positions based on the transfer function (it is reasonable to assume a rigid Z axis, so no model is needed for force/vibration in that direction). The model can be adjusted to reflect the 4 different configurations of the boom by loading the corresponding transfer function parameters.

For example, we show the process of creating a transfer function model under Configuration 1 using the data measured by the accelerometer at point A and the impact hammer when hitting close to point A. For a better fitting outcome with an appropriate number of poles and zeros, the most significant,

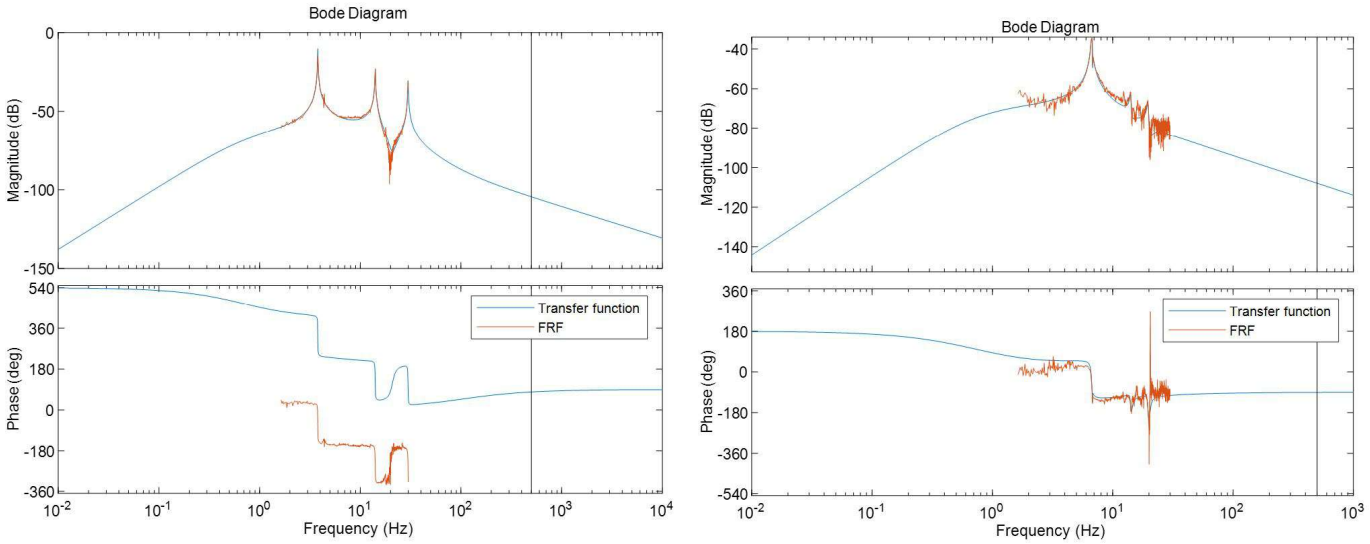

(a) Vertical model: data measured by the accelerometer at point A and the impact hammer when hitting close to point A.

(b) Horizontal model: data measured by the accelerometer at point B and the impact hammer when hitting close to point B.

Fig. 4: Bode plot of the modified transfer function models against their FRFs under Configuration 1.

and reliable FRF data were extracted, i.e., we focus on the range 1 – 50 Hz where the vibration is well-defined by its first modal frequencies (the FRFs are calculated from the selected resonances' data, including valuable dynamics information). We use the Matlab command "*tfest*" to fit the data with 10 poles and 9 zeros, followed by a minor pole-zero modification for the model to be stable. Fig. 4 presents the Bode plots of such a modified transfer function model for point A (vertical) as Fig. 4a and also the one for point B (horizontal) as Fig. 4b[1]. The same process is repeated for the other three configurations, which leads to eight transfer functions in total. The model's fidelity is validated by computing the relative error $\mathrm{RE}(j\omega) = \|\mathrm{Model}(j\omega) - \mathrm{Data}(j\omega)\| / \|\mathrm{Model}(j\omega)\|$, which keeps around 1% in average for all frequency points. This provides us with transfer function models $\boldsymbol{T}_i = \boldsymbol{a}/\boldsymbol{f}$ relating the forces $\boldsymbol{f}$ at the base to the acceleration $\boldsymbol{a}$, modelling all the significant resonances. A feedback controller needs to be able to compensate for those resonances, while the H_∞ design allows to define an uncertainty model of the transfer function outside that focused frequency region of 1-50 Hz.

III. Control Design

The above section has provided a detailed insight into the interaction dynamics of the robot manipulator with the flexible long-reach boom. The understanding of these dynamics, i.e., the impact of the manipulator on the boom end point vibrations, is instrumental in reducing any vibrations at the boom end. This has been shown to perform well in our earlier work on *trajectory planning*, i.e., open-loop/feedforward strategies [38]. The next step of this work is to demonstrate the active damping of vibrations at the end of the boom through closed-loop/feedback control. Inertia sensing would feed back acceleration measurements from the end of the boom to the controller, which would command the robot to suppress the boom end's vibrations whilst following the planned path trajectories as closely as possible.

A. Control Strategy Overview

A closed-loop control scheme for this application requires reliable real-time capabilities of both the controller and the commercial robotic system such as the Doosan Robotics Cobot M1013. Controlling the joints of the robot requires joint velocity actuation at a specific update rate with limited time jitter and delay. We determined the resonance frequency of approximately 30 Hz based on experimental modal analysis results, which identified three dominant modal frequencies at 3.8 Hz, 14.1 Hz, and 29.8 Hz. Given that the largest significant resonance frequency of the boom system is close to 30 Hz, the update rate needs to be higher than 2×30 Hz $=$ 60 Hz. Any jitter needs to be significantly less than $1/60$ s $\approx$ 16.7 ms, with a delay in the order of 16.7 ms or ideally significantly less. In addition, the control system has to integrate inertia sensing and computing a control action within a period significantly less than 16.7 ms.

The main nonlinearities in this case are those from the robot manipulator dynamics; the nonlinearities are therefore readily captured in a model of smooth functions. Under the reasonable assumption of the motion of the manipulator joint in an envelope of a nominal (possibly straight) arm operating position, the control can be achieved via a linearized representation in a sufficiently wide envelope of the nominal manipulator position (as demonstrated). In the context of the TWD system, H_∞ control is particularly advantageous due to its ability to suppress multi-modal vibrations and handle structural flexibilities inherent in the boom. It will be seen that H_∞ control is powerful enough to deal with the nominal straight position and a wider envelope of joint demands, i.e.,

[1]The 540° and 180° in the Bode phase plots of Fig. 4 can be explained by the roll-up rate of the magnitude plot due to the relation between acceleration and position.

the H_∞ controller will augment and enhance the nominal inbuilt joint control system, ensuring the original controller continues to function. The actual level of effectiveness in light of the nonlinearities is a complex connection between the designed controller and the prevalent nonlinearities. This sets the precedent for further work where, for instance, a *gain-scheduling* flexible controller [39] can deal with the complete nonlinearities and workspace of the manipulator within the TWD system.

B. Mixed-Sensitivity H_∞ Synthesis

The model for flexible control design is computed from the "Model Linearizer" of the simulation model in Matlab/Simulink. The results of the closed-loop controller will demonstrate results in a reliably large envelope of the starting position, considering that here the nonlinear dynamics are those dominated by the robot manipulator. Note that the Matlab/Simscape model employs a local *proportional-differential* (PD) joint velocity controller of high bandwidth; the interaction/ground forces at the base of the horizontally placed robot manipulator are measured in the lateral directions of the base, i.e., in the vertical and horizontal directions. These forces are inputs into the transfer functions for the flexible boom vibration models, i.e., the force to acceleration transfer function which was initially measured and included into the simulation to reflect the boom flexibilities. Hence, the "*Model Linearizer*" is used to derive the transfer function, with its inputs as the position demand of the 2nd and 3rd rotational joints, and its outputs as the horizontal and vertical acceleration of the boom vibration model, and the positions of the two above-mentioned degrees of freedom.

We focus on the possible excitation of the boom flexibilities in the horizontal plane for which the 2nd and 3rd rotational degrees are sufficient to actively compensate for those flexible modes, should they have been excited by disturbances. Therefore, we are using the two most effective rotational joints delivering the highest effective actuation force, in particular also in the direction of the investigated vertical boom acceleration.

The two-input, four-output model is given by

$$\begin{bmatrix} \boldsymbol{a}(s) \\ \boldsymbol{q}(s) \end{bmatrix} = \begin{bmatrix} \boldsymbol{T}_a(s) \\ \boldsymbol{T}_q(s) \end{bmatrix} \boldsymbol{q}_d(s), \tag{1}$$

where $\boldsymbol{a}(s)$ denotes the two orthogonal boom-end accelerations (horizontal and vertical), $\boldsymbol{q}(s)$ represents the joint position vector of two rotational degrees of freedom, and $\boldsymbol{q}_d(s)$ is the corresponding demand vector. This provides the two transfer function matrices $\boldsymbol{T}_a(s)$ and $\boldsymbol{T}_q(s)$, via the relationships of $\boldsymbol{a}(s) = \boldsymbol{T}_a(s)\boldsymbol{q}_d(s)$ and $\boldsymbol{q}(s) = \boldsymbol{T}_q(s)\boldsymbol{q}_d(s)$. These are being used to design a two-degree-of-freedom feedforward and feedback controller, which establishes

$$\boldsymbol{q}_d(s) = \boldsymbol{C}_q(s)\boldsymbol{q}_{dd}(s) + \boldsymbol{C}_a(s)\boldsymbol{a}(s), \tag{2}$$

where $\boldsymbol{C}_q(s)$ is the feedforward component for a demand trajectory $\boldsymbol{q}_{dd}(s)$ for the 2nd and 3rd rotational degree, while $\boldsymbol{C}_a(s)$ is the feedback component using the horizontal and vertical acceleration signals, forming the vector $\boldsymbol{a}(s)$. Here $\boldsymbol{C}_q(s)$ and $\boldsymbol{C}_a(s)$ are to be designed through the H_∞ controller for feedforward of the demand trajectory $\boldsymbol{q}_{dd}$ (e.g. the optimised polynomial trajectory in [38]) and feedback of the measured boom acceleration $\boldsymbol{a}(s)$. Hence, the objective of the controller is for the acceleration $\boldsymbol{a}(s)$ to be minimized while following $\boldsymbol{q}_{dd}(s)$ up to a certain bandwidth.

The transfer function Bode plots for the model of $[\boldsymbol{T}_a(s)\ \ \boldsymbol{T}_q(s)]^\mathsf{T}$ are presented in Fig. 5. The selected frequency range (10^0–10^4 rad/s) captures both low-frequency joint motion and higher-frequency flexible mode resonances. In particular, $\boldsymbol{T}_a(s)$ highlights resonance amplification while $\boldsymbol{T}_q(s)$ confirms the high-bandwidth response of the manipulator joint actuation. It is vital to note in Fig. 5a, the significant gain increase of more than 40 dB/dec below 20 rad/s, while the resonances at 3.8 Hz (23.9 rad/s) and specifically at 14.1 Hz (88.6 rad/s) and 29.8 Hz (187.2 rad/s) are highly pronounced due to the significant increase in gain. Thus, the double/triple temporal derivative (acceleration or jerk) of the joint position motion is to be detected at the boom end in terms of the acceleration measurements at the boom. The forces and torques at the base of the robot manipulator reflect the acceleration or jerk of the robot manipulator's joint positions. This is a key result and crucial motivation for any optimization of the joint motion of the robot manipulator. The results of Fig. 5b are largely expected. They reflect the high bandwidth behavior of the transfer function, where the transfer function resembles largely an identity matrix for a frequency of up to 1000 rad/s. Note that this is an idealized simulation, and the practical implementation bandwidth of the commercial controller would have to be verified.

The objective of the H_∞ control problem for $\boldsymbol{q}(s)$ is to follow $\boldsymbol{q}_{dd}(s)$ while avoiding high amplitudes of $\boldsymbol{a}(s)$ in the time domain. Hence, the design problem is represented in Fig. 6.

Here, the controller design parameters are determined by the lag filter

$$\boldsymbol{W}_q(s) = \frac{s/w + g_{\max}}{s/w + 1} \begin{bmatrix} 1 & 0 \\ 0 & 1 \end{bmatrix}, \tag{3}$$

which creates a low-frequency performance constraint for $g_{\max} = 10$ and $w = 1/\sqrt{10}$, specifically for the feedforward compensator $\boldsymbol{C}_q(s)$. Evidently, $\boldsymbol{z}_1(s)$ is a design performance output, the frequency-weighted joint path error. The constant weight

$$\boldsymbol{W}_a(s) = \frac{1}{10} \begin{bmatrix} 1 & 0 \\ 0 & 1 \end{bmatrix}, \tag{4}$$

is a boom-end acceleration constraint to keep the magnitude of $\boldsymbol{a}(s)$ low, i.e., to reduce vibrations. Thus, $\boldsymbol{z}_2(s)$ is another design performance output, the weighted boom acceleration vector. An increase of the gain for $\boldsymbol{W}_a(s)$ will reduce the acceleration $\boldsymbol{a}(s)$. However, a too-large value will force significant control changes in $\boldsymbol{q}_d$ for acceleration compensation which is undesirable. In design, one usually introduces a small weight and observes the impact and changes on the boom acceleration with the different iterations of the design of the controller $[\boldsymbol{C}_q(s)\ \ \boldsymbol{C}_a(s)]$. Note that the resonance in $\boldsymbol{T}_a(s)$ is *highly pronounced* in Fig. 5a, i.e., the optimization targets indeed that resonance. The weight of

$$W_n(s) = 0.00001 \frac{s/w_n + g_n}{s/w_n + 1} \begin{bmatrix} 1 & 0 \\ 0 & 1 \end{bmatrix}, \tag{5}$$

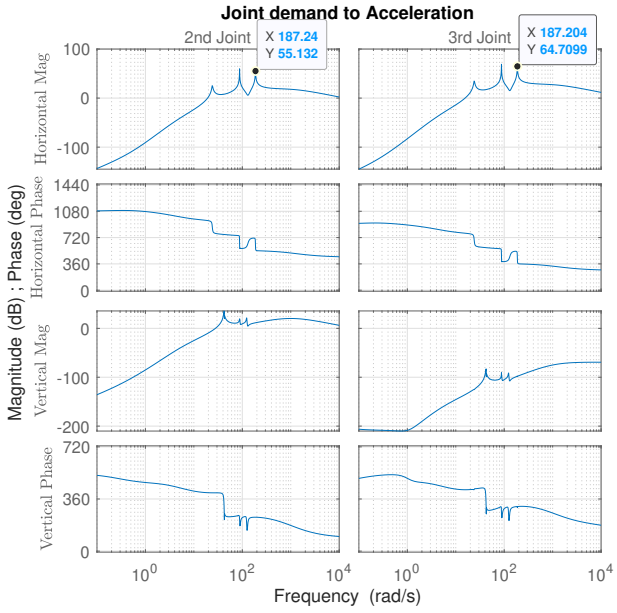

(a) Bode plots of $\boldsymbol{T}_a(s)$: Position demand of the 2nd and 3rd rotational joints (left and right column respectively) to the horizontal and vertical accelerations (top 2 and bottom 2 rows respectively).

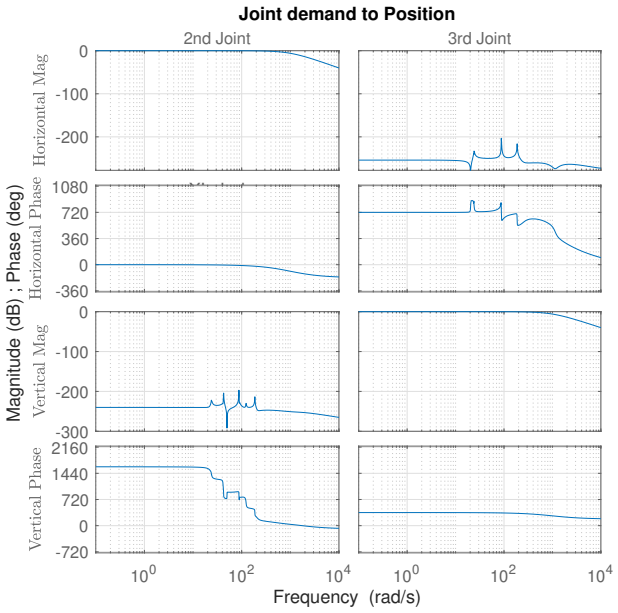

(b) Bode plots of $\boldsymbol{T}_q(s)$: Position demand of the 2nd and 3rd rotational joints (left and right column respectively) to their relevant actual positions (top 2 and bottom 2 rows respectively).

Fig. 5: Bode plots of the transfer functions $\boldsymbol{T}_a(s)$ and $\boldsymbol{T}_q(s)$.

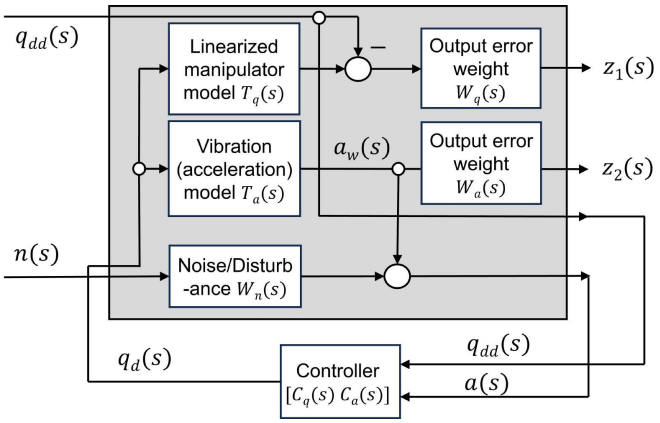

Fig. 6: Mixed Sensitivity design problem using H_∞ control.

with the values $g_n = 100$ and $w_n = 9$ is practically motivated; it acts to limit the gain of $\boldsymbol{C}_a(s)$, modeling uncertainty and noise $\boldsymbol{n}(s)$ in the measurement of the acceleration vector $\boldsymbol{a}(s)$. Therefore, the noise/disturbance $\boldsymbol{n}(s)$ does not necessarily practically exist; it helps to shape the controller $\boldsymbol{C}_a(s)$ the weight $W_n(s)$.

IV. Real-Time Implementation based on Joint Velocity Control

High-level functionality for the Doosan Robotics Cobot M1013 is limiting the sampling rates of the robot manipulator to two different rates 70 Hz and 500 Hz, where the first maximal update rate is available to joint position actuation and the faster maximal update rate to joint velocity actuation. Assuming a 70 Hz sampling frequency, we tested the control approach from Section III.B (see also the Appendix for the design). The tests resulted in poor performance due to the low sampling frequency. Hence, an improved controller is to be deployed using a 500 Hz update rate. Joint velocity corrections from the H_∞ controller are sent to the manipulator via a TCP/IP interface with negligible communication delay. The entire control pipeline runs in hard real-time, ensuring consistent loop latency for reliable vibration attenuation. The discrete-time control design is synthesized based on the experimentally identified models to allow operation using only joint velocity actuation and feedback from boom acceleration, joint velocity, and joint position. This is to reflect the practical constraints of the commercial robots and differentiates this approach from classical torque-based implementations. The discrete-time implementation is designed to suppress dominant vibration modes and tolerate the nonlinear coupling between the manipulator and boom dynamics without requiring nonlinear compensation (The discrete-time controller design process follows the same process as in the Appendix).

The objective of the H_∞ control problem for $\boldsymbol{q}(s)$ is to follow $\boldsymbol{q}_{dd}(s)$ while avoiding high amplitudes of $\boldsymbol{a}(s)$ in the time domain. The modified H_∞ control design is detailed in Fig. 7. The output used for feedback signals is the demand joint position $\boldsymbol{q}_{dd}(s)$, the actual joint position $\boldsymbol{q}(s)$, the actual joint velocity $\dot{\boldsymbol{q}}(s)$, and the acceleration at the end of boom $\boldsymbol{a}(s)$. The control input is the demand joint velocity $\dot{\boldsymbol{q}}_d(s)$.

Control is achieved through a demand for joint velocity $\dot{\boldsymbol{q}}_d(s)$. Thus, the plant is in this case,

$$\begin{bmatrix} \boldsymbol{q}(s) \\ \dot{\boldsymbol{q}}_w(s) \\ \boldsymbol{a}_w(s) \end{bmatrix} = \begin{bmatrix} \tilde{\boldsymbol{T}}_{qp}(s) \\ \tilde{\boldsymbol{T}}_{qv}(s) \\ \boldsymbol{T}_a(s)/s \end{bmatrix} \dot{\boldsymbol{q}}_d(s), \tag{6}$$

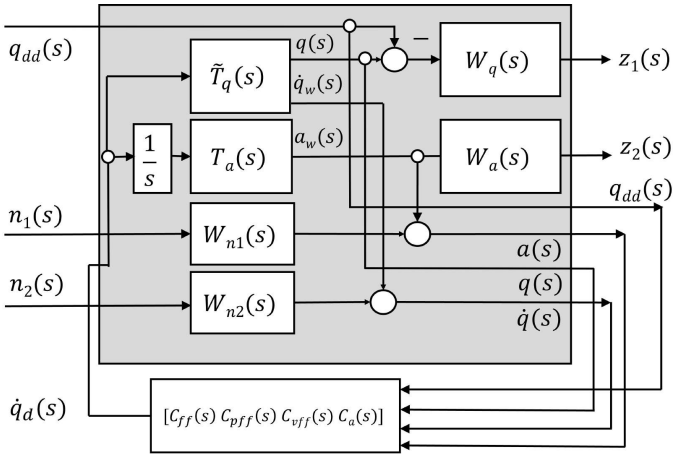

Fig. 7: Modified mixed-sensitivity design using H_∞ control for joint velocity-based actuation.

where $\tilde{\boldsymbol{T}}_q(s) = \begin{bmatrix}\tilde{\boldsymbol{T}}_{qp}(s) & \tilde{\boldsymbol{T}}_{qv}(s)\end{bmatrix}^\mathsf{T}$ denotes the transfer functions to joint position $\boldsymbol{q}(s)$ and joint velocity $\dot{\boldsymbol{q}}_w(s)$ (without noise/uncertainty impact). The plant is derived from the linearization of the dynamics model using a velocity actuation principle for only the 2nd and 3rd rotational joints of the robot manipulator (it is vital to understand that it is 2nd and 3rd joints that rotate the two big links of the manipulator with major mass). Note that $\boldsymbol{T}_a(s)/s$ is the transfer function from the joint velocity demand to the boom end acceleration measurement $\boldsymbol{a}_w(s)$ (without noise and disturbance). Therefore, the controller has an extended structure:

$$\dot{\boldsymbol{q}}_d(s) = \begin{bmatrix}\boldsymbol{C}_{ff}(s) & \boldsymbol{C}_{pff}(s) & \boldsymbol{C}_{vff}(s) & \boldsymbol{C}_a(s)\end{bmatrix} \begin{bmatrix}\boldsymbol{q}_{dd}(s)\\ \boldsymbol{q}(s)\\ \dot{\boldsymbol{q}}(s)\\ \boldsymbol{a}(s)\end{bmatrix}, \tag{7}$$

where $\dot{\boldsymbol{q}}(s)$ is the joint velocity (with noise/uncertainty impact) and $\boldsymbol{a}(s)$ the boom end acceleration measurement (with noise and disturbance).

As before the controller design parameters are determined by: $\boldsymbol{W}_q(s)$ is the same value as (3), and

$$\boldsymbol{W}_a(s) = 2\begin{bmatrix}1 & 0\\ 0 & 1\end{bmatrix}, \tag{8}$$

$$\boldsymbol{W}_{n1}(s) = 10^{-5}\left(\frac{s/w_1+g_1}{s/w_1+1} + \frac{s/w_2+1}{s/w_2+g_2}\right)\begin{bmatrix}1 & 0\\ 0 & 1\end{bmatrix}, \tag{9}$$

with the values $g_1 = 100$, $w_1 = 9$, $g_2 = 1000$, and $w_2 = 20/\sqrt{10}$ is to limit the gain of $\boldsymbol{C}_a(s)$, modeling uncertainty and noise $\boldsymbol{n}_1(s)$ in the measurement of the acceleration vector $\boldsymbol{a}(s)$. Similarly, the noise/disturbance $\boldsymbol{n}_1(s)$ does not necessarily practically exist; as part of a multiplicative uncertainty model, it helps to shape the controller $\boldsymbol{C}_a(s)$, the weight $\boldsymbol{W}_{n1}(s)$ keeping their gain lower in low and high frequency, while the mid-frequency range, i.e. at the resonant modes, has an active control element $\boldsymbol{C}_a(s)$. The feedback controller requires the control of the joint position as velocity $\dot{\boldsymbol{q}}_d(s)$ is used to actuate the robot manipulator. Hence, we need to assume that the joint velocity measurement is subject to noise $\boldsymbol{n}_2(s)$, with the following frequency spectrum:

$$\boldsymbol{W}_{n2}(s) = 0.01\begin{bmatrix}1 & 0\\ 0 & 1\end{bmatrix}, \tag{10}$$

which is to limit the gain of $\boldsymbol{C}_{vff}(s)$, modeling uncertainty and noise $\boldsymbol{n}_2(s)$ related to the joint velocity vector $\dot{\boldsymbol{q}}(s)$ measurement.

The mixed sensitivity design problem can therefore be expressed as

$$\begin{bmatrix}\boldsymbol{z}_1(s)\\ \boldsymbol{z}_2(s)\\ \boldsymbol{q}_{dd}(s)\\ \boldsymbol{q}(s)\\ \dot{\boldsymbol{q}}(s)\\ \boldsymbol{a}(s)\end{bmatrix} = \begin{bmatrix}-\boldsymbol{W}_q & 0 & 0 & \boldsymbol{W}_q\tilde{\boldsymbol{T}}_{qp}\\ 0 & 0 & 0 & \boldsymbol{W}_a\boldsymbol{T}_a/s\\ \boldsymbol{I} & 0 & 0 & 0\\ 0 & 0 & 0 & \tilde{\boldsymbol{T}}_{qp}\\ 0 & 0 & \boldsymbol{W}_{n2} & \tilde{\boldsymbol{T}}_{qv}\\ 0 & \boldsymbol{W}_{n1} & 0 & \boldsymbol{T}_a/s\end{bmatrix}\begin{bmatrix}\boldsymbol{q}_{dd}(s)\\ \boldsymbol{n}_1(s)\\ \boldsymbol{n}_2(s)\\ \dot{\boldsymbol{q}}_d(s)\end{bmatrix} \tag{11}$$

where the vector $\begin{bmatrix}\boldsymbol{q}_{dd}(s) & \boldsymbol{n}_1(s) & \boldsymbol{n}_2(s) & \dot{\boldsymbol{q}}_d(s)\end{bmatrix}^\mathsf{T}$ feeds into the controller (7) for $\dot{\boldsymbol{q}}_d(s)$. Robustness to modeling uncertainties, including resonance frequency shifts and unmodeled nonlinearities, is addressed through the frequency shaping in the H_∞ synthesis. The weighting functions are selected to achieve gain roll-off beyond the dominant flexible modes while maintaining performance around the primary resonance frequencies, ensuring stability under expected deviations. The discrete controller is designed at 500 Hz (see Appendix) and reduced to 30th order.

This design process and the use of the bilinear transformation are commonly employed in the design of discrete-time mixed-sensitivity controllers [40]. The feedback loop uses acceleration measurements to detect unwanted oscillations, and the controller injects corrective joint velocity commands to counteract them in real time. This shaping is done in the frequency domain, allowing the controller to precisely target dominant resonant modes while respecting bandwidth limits.

V. Results

This section presents the simulation and experimental results of the proposed TWD system controller, followed by a discussion on its robustness.

A. Simulations

To demonstrate the effectiveness of the controller, 2nd and 3rd rotational joints of the robot manipulator were controlled to move from home to the demand positions, respectively. The trajectories for 2 joints started when the manipulator was stationary, ensuring no initial vibration. The step input was used to simulate the occurrence of transient disturbances. This discontinuous demand causes significant boom vibrations which are to be actively dampened by the proposed controller. To be specific, the 2nd joint moves from 0 to 5 degrees, and the 3rd joint moves from 0 to -5 degrees at the same time (The choice was made based on the observation of the vibration in the real system to meet the safety requirement. The results are representative since the 2nd and 3rd joints rotate the two major links that carry the most weight). This shows that the nominal

joint controller remains intact, while the vibration-damping scheme is used.[2]

In the simulation results, it is found that the proposed controller effectively rejects vibrations under disturbance for all four boom configurations. Fig. 8 shows the simulated vertical acceleration response under Configuration 1. The closed-loop controller effectively mitigated vibrations following the step disturbance, with a significant reduction beginning around 1.7 seconds. In Configuration 1, the simulation achieved a peak amplitude of 0.14 g, demonstrating a significant reduction in vibration compared to the experimental result (0.19 g). The average vibration reduction reached 91%, indicating highly effective attenuation of oscillations.

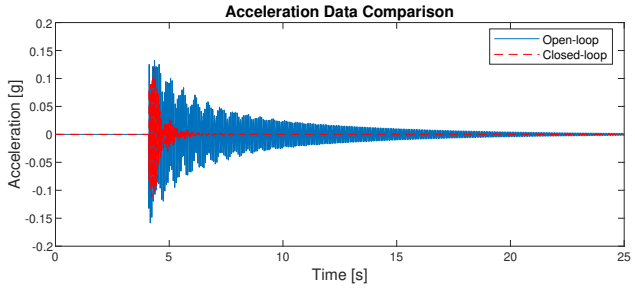

Fig. 8: Simulated vertical acceleration results.

While the dominant resonance frequencies observed in simulation and experiment are consistent, the simulation exhibits additional high-frequency components that are not present in the real system. These arise due to the absence of damping and compliance in the simulation model, which allows higher-order modes to persist without suppression.

B. Experiments

To implement the above velocity-based controller on the Doosan Robotics Cobot M1013, we employed "*speedj_rt*" and obtained control implementation at a sampling rate of 500 Hz. We utilize an *inertial measurement unit* (IMU) for inertial sensing, i.e., the acceleration measurement for real-time feedback. To validate the proposed controller, we carried out the experiments the same way as the simulations above. Fig. 9 shows the acceleration measurements when the closed-loop controller is enabled under Boom Configuration 1[3]. Specifically, the reduction in vibration amplitude begins immediately and becomes significant after approximately 1 s. Fig. 10 provides a visual comparison of the vibration suppression effect by showing the position of the laser dot projected onto a canvas by the end-effector-mounted laser device. The snapshots, taken at two time instants ($t = 5.14$ s and $t = 5.23$ s), illustrate the difference between the open-loop case (top row) and the proposed closed-loop H_∞ control (bottom row). The laser dot under closed-loop control exhibits significantly reduced motion.

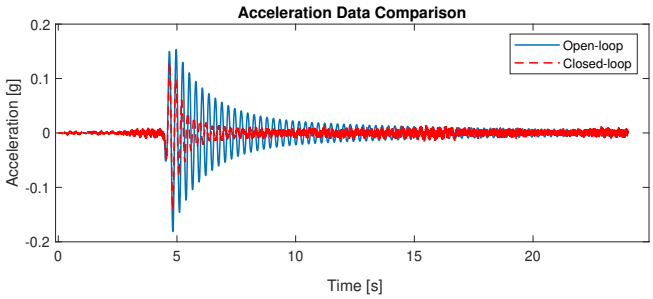

Fig. 9: Experimental vertical acceleration results.

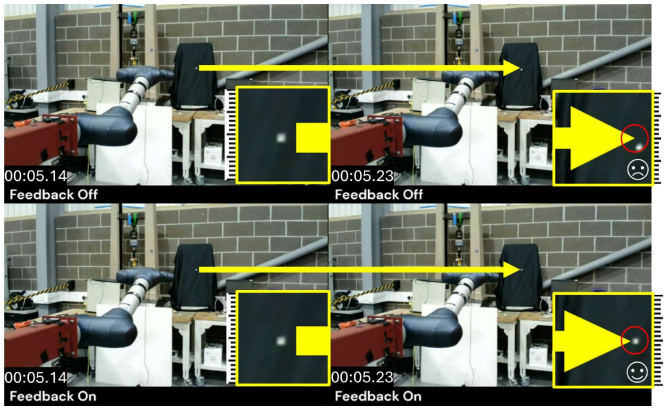

Fig. 10: Experimental comparison of laser dot position at different time instants: $t = 5.14$ s (Left column) and $t = 5.23$ s (Right column): *Open-loop* case (Top row) v.s. *Closed-loop* control (Bottom row).

In the experimental results[4], the feedback controller can effectively follow the positional demand and reject disturbance. Table II summarizes the comparison between the simulations and experiments, showing the vibration reduction with around 80% on average achieved by the proposed control. The results demonstrate that our H_∞ controller effectively suppressed vibrations across multiple configurations, which implies its robustness against variations in system dynamics. While peak acceleration is not drastically reduced in all cases due to the timing of motion-induced impulses, the proposed controller rapidly suppresses residual oscillations. This is reflected in the significant reduction in RMS acceleration and lead time. The control law acts on the flexible dynamics excited post-motion, effectively shortening the vibration tail even if the initial transient remains.

Practical results of joint angle changes for the 2$^{\text{nd}}$ joint from 0 to 5, 10, 30 degrees, and the 3$^{\text{rd}}$ joint moves from 0 to -5, -10, -30 degrees at the same time show in terms of vibration suppression consistent results for increasing angular steps, while also providing practical proof for the designed robustness of the vibration damping controller and the capability for the nominal joint control to work, as designed [4].

[2]Practically, we have tested this approach for this and larger angular changes, i.e. $\{\pm 5^\circ, \pm 10^\circ, \pm 30^\circ\}$

[3]Comparing Fig. 9 against Fig. 8, the discrepancy between simulation and experimental results can be attributed to (i) the high-bandwidth, data-capture hardware used in model analysis experiments which allows for (ii) high-bandwidth simulated models together with practical consideration for sampling creating a very differentiated numerical simulation system in contrast to (iii) the practical, Doosan-provided control hardware used for closed-loop control, which limits detail during real-time data capture.

[4][Online] Video available via the url: https://youtu.be/3HQk8qZHFpA

TABLE II: Vibration reduction results. Peak = Peak Acceleration (g), RMS = Root Mean Square (g), Avg. Red. = Average Reduction (%), Lead Time (s). The *peak amplitude* denotes the maximum absolute value of the acceleration; the *average reduction* is computed based on the squared RMS (i.e., energy) of both horizontal and vertical accelerations: $1-(\mathrm{RMS}^2_{\mathrm{Closed}}/\mathrm{RMS}^2_{\mathrm{Open}})$; the *lead time* is defined as the time to reach the 70% amplitude reduction envelope from the onset of robot motion.

Config.	Open-loop		Closed-loop		Avg.	Lead
	Peak	RMS	Peak	RMS	Red. (%)	Time (s)
1 (Sim)	0.42	0.23	0.14	0.07	91	0.85
2 (Sim)	0.38	0.23	0.13	0.06	93	1.15
3 (Sim)	0.41	0.25	0.14	0.07	92	1.20
4 (Sim)	0.34	0.16	0.07	0.05	90	1.05
Avg (Sim)	0.39	0.22	0.12	0.06	91.5	1.06
1 (Exp)	0.48	0.24	0.19	0.12	75	1.12
2 (Exp)	0.43	0.24	0.18	0.10	83	1.45
3 (Exp)	0.44	0.24	0.19	0.10	83	1.50
4 (Exp)	0.36	0.17	0.10	0.08	79	1.29
Avg (Exp)	0.43	0.22	0.17	0.10	80	1.34

C. Discussion

Despite the complexity of the underlying model, the implemented controller of 30th order operates at 500 Hz in real time using only joint velocity actuation, confirming its computational suitability for embedded industrial systems. The proposed controller is designed to effectively handle multi-modal flexibilities, meaning it can address a set of resonance frequencies in the boom. It exhibits robust performance under moderate changes in resonance frequencies. However, a re-design may be necessary for significant resonance shifts, such as those caused by changes in boom configurations. To address this, the gain scheduling schemes discussed earlier are recommended for accommodating dynamic changes across different boom configurations. While the current experiments focus on representative real-world configurations, the proposed control framework is compatible with more dynamic scenarios. For example, trajectory optimization for vibration mitigation under high-speed motions has been demonstrated in our earlier work [38], which can be combined with the present feedback controller to further enhance performance in aggressive tasks.

1) Comparison Between Velocity-Based and Position-Based Controllers: Although the velocity-based controller was implemented in this study, the initial position-based controller remains a suitable alternative solution, provided it operates within the real-time capabilities of the robot. The position-based controller typically functions at a control rate below 100 Hz and is designed for discrete-time operation. In contrast, the velocity-based controller can operate at a higher frequency, enabling more precise vibration control.

2) Frequency Region of Controller Activity and Robustness: The proposed flexible control method activates the closed-loop controller only within the frequency region corresponding to the boom's resonance frequencies. This is achieved by ensuring sufficient roll-off at both low and high frequencies, effectively suppressing vibrations outside the resonance band. This behavior results from introducing the uncertainty weighting function $\boldsymbol{W}_n(s)$, which, together with $\boldsymbol{W}_a(s)$, forms a multiplicative uncertainty model. The weighting function $\boldsymbol{W}_n(s)$ has a high gain at low frequencies below the resonance band, enforcing the desired roll-off behavior.

3) Feedback Controller Robustness Against Model Uncertainties: The robustness of the feedback controller against resonance model uncertainties is ensured by maintaining lower gains outside the resonance frequencies. This robustness is further reinforced at low frequencies due to the joint position-to-acceleration relationship, which can be approximated as: $\boldsymbol{a}(s) \approx s^2 \boldsymbol{M}\boldsymbol{T}_i(s)\boldsymbol{L}(s)\boldsymbol{q}_d(s)$, where $\boldsymbol{a}(s)$ is the boom acceleration measured from the impact hammer force $\boldsymbol{F}(s)$ via $\boldsymbol{T}_i(s)$, and $\boldsymbol{L}(s)$ is a low-pass filter representing the internal joint position control loop with $\boldsymbol{L}(0)=\boldsymbol{I}$. The constant matrix $\boldsymbol{M}$ relates to the robot manipulator's parameters. This relationship introduces a natural low gain in $\boldsymbol{T}_a(s)$ due to the s^2 term at low frequencies (as also noticed in Section III.B), thereby providing inherent robustness to the open-loop response.

VI. Conclusion

In this paper, we have shown that the proposed controller mitigated vibrations effectively in both simulations and experiments, specifically, the modified velocity-based controller can reduce vibration by 80% on average. The study demonstrates that the proposed control can be effectively embedded into commercial joint-velocity actuated manipulators in challenging industrial environments, e.g. also for the Fukushima Daiichi site, enabling dynamic model-based vibration suppression without hardware modification. For broader applications and future work, one might take care of sample delays, which can be built-in by investigating for such delays and multiplying multiple of $1/z$ to the discrete plant model, as needed. Possible alternatives to the ZOH discretization can be tested, e.g., first-order hold (FOH) due to its interpolation.

Appendix
Design of a Discrete-Time H_∞ Controller

Given the design problem stated in Fig. 6, the controller design follows a discrete-time approach as advocated in [34], [40]. This is necessary due to the limited sampling frequency available for the practical implementation of any closed-loop strategy on the robot manipulator. Assuming 70 Hz update rate is available and following the setup of the design problem in Fig. 6, the key steps are:

1) Create the augmented transfer function model, $\boldsymbol{T}_{\mathrm{aug}}(s)$, for the mixed-sensitivity problem:

$$\begin{bmatrix} \boldsymbol{z}_1(s) \\ \boldsymbol{z}_2(s) \\ \boldsymbol{q}_{dd}(s) \\ \boldsymbol{a}(s) \end{bmatrix} = \boldsymbol{T}_{\mathrm{aug}}(s) \begin{bmatrix} \boldsymbol{q}_{dd}(s) \\ \boldsymbol{n}(s) \\ \boldsymbol{q}_d(s) \end{bmatrix}, \tag{12}$$

where

$$\boldsymbol{T}_{\mathrm{aug}}(s) = \begin{bmatrix} -\boldsymbol{W}_q(s) & 0 & \boldsymbol{W}_q(s)\boldsymbol{T}_q(s) \\ 0 & 0 & \boldsymbol{W}_a(s)\boldsymbol{T}_a(s) \\ \boldsymbol{I} & 0 & 0 \\ 0 & \boldsymbol{W}_n(s) & \boldsymbol{T}_a(s) \end{bmatrix}. \tag{13}$$

2) Apply a zero-order hold (ZOH) transformation at 70 Hz to get $\boldsymbol{T}_{\mathrm{aug,zoh}}(z)$.

3) Use a bilinear transformation (Tustin's method) to map $\boldsymbol{T}_{\text{aug,zoh}}(z)$ to a continuous-time transfer function $\boldsymbol{T}_{\text{aug,bil}}(s)$.
4) Perform $\mathscr{H}_\infty$ synthesis on $\boldsymbol{T}_{\text{aug,bil}}(s)$ to obtain $\begin{bmatrix}\boldsymbol{C}_{q,\text{bil}}(s) & \boldsymbol{C}_{a,\text{bil}}(s)\end{bmatrix}$.
5) Convert the controller back to the discrete domain via inverse bilinear transform to get $\begin{bmatrix}\boldsymbol{C}_{q,\text{zoh}}(z) & \boldsymbol{C}_{a,\text{zoh}}(z)\end{bmatrix}$.

REFERENCES

[1] K. Zhang, A. Plianos, L. Raimondi, F. Abe, Y. Sugawara, I. Caliskanelli, A. Cryer, J. Thomas, S. Pacheco-Gutierrez, C. Hope *et al.*, "Towards safe, efficient long-reach manipulation in nuclear decommissioning: a case study on fuel debris retrieval at fukushima daiichi," *Journal of Nuclear Science and Technology*, vol. 62, no. 1, pp. 1–16, 2025.

[2] B. Siciliano, L. Sciavicco, L. Villani, and G. Oriolo, *Robotics: Modelling, Planning and Control*, ser. Advanced Textbooks in Control and Signal Processing. Springer, 2009.

[3] A. Billard and D. Kragic, "Trends and challenges in robot manipulation," *Science*, vol. 364, no. 6446, p. eaat8414, 2019.

[4] M. A. Roa, M. R. Dogar, J. Pages, C. Vivas, A. Morales, N. Correll, M. Gorner, J. Rosell, S. Foix, R. Memmesheimer *et al.*, "Mobile manipulation hackathon: Moving into real world applications," *IEEE Robotics & Automation Magazine*, vol. 28, no. 2, pp. 112–124, 2021.

[5] S. Erhart, D. Sieber, and S. Hirche, "An impedance-based control architecture for multi-robot cooperative dual-arm mobile manipulation," in *2013 IEEE/RSJ International Conference on Intelligent Robots and Systems (IROS)*. IEEE, 2013, pp. 315–322.

[6] Y. Liu, Z. Li, H. Su, L. Jiang, and C.-y. Su, "Whole body control of an autonomous mobile manipulator using series elastic actuators," *IEEE/ASME Transactions on Mechatronics*, 2021.

[7] K. A. Tahboub, "Intelligent control for manipulators with moving bases," *Journal of Intelligent Manufacturing*, vol. 9, no. 1, pp. 1–7, 1998.

[8] Y. Liu, X. Chen, Y. Mei, and Y. Wu, "Observer-based boundary control for an asymmetric output-constrained flexible robotic manipulator," *Science China. Information Sciences*, vol. 65, no. 3, p. 139203, 2022.

[9] Y. Li, S. S. Ge, Q. Wei, T. Gan, and X. Tao, "An online trajectory planning method of a flexible-link manipulator aiming at vibration suppression," *IEEE Access*, vol. 8, pp. 130 616–130 632, 2020.

[10] Z. Qiu, C. Li, and X. Zhang, "Experimental study on active vibration control for a kind of two-link flexible manipulator," *Mechanical Systems and Signal Processing*, vol. 118, pp. 623–644, 2019.

[11] Z. Mohamed, J. Martins, M. Tokhi, J. S. Da Costa, and M. Botto, "Vibration control of a very flexible manipulator system," *Control Engineering Practice*, vol. 13, no. 3, pp. 267–277, 2005.

[12] A. Takata and G. Endo, "Dynamics-based control and path planning method for long-reach coupled tendon-driven manipulator," *Journal of Robotics and Mechatronics*, vol. 36, no. 1, pp. 30–38, 2024.

[13] Y. Meng, G. Fang, J. Yang, Y. Guo, and C. C. Wang, "Spring-IMU fusion-based proprioception for feedback control of soft manipulators," *IEEE/ASME Transactions on Mechatronics*, 2023.

[14] F. Xu, Y. Zhang, J. Sun, and H. Wang, "Adaptive visual servoing shape control of a soft robot manipulator using bezier curve features," *IEEE/ASME Transactions on Mechatronics*, vol. 28, no. 2, pp. 945–955, 2022.

[15] B. Li, X. Li, H. Gao, and F.-Y. Wang, "Advances in flexible robotic manipulator systems—part I: Overview and dynamics modeling methods," *IEEE/ASME Transactions on Mechatronics*, 2024.

[16] K. Lochan, B. K. Roy, and B. Subudhi, "A review on two-link flexible manipulators," *Annual Reviews in Control*, vol. 42, pp. 346–367, 2016.

[17] X. Chen and T. Fukuda, "Robust sliding-mode tip position control for flexible arms," *IEEE Transactions on Industrial Electronics*, vol. 48, no. 6, pp. 1048–1056, 2001.

[18] Y. Lin, Z. Chen, and B. Yao, "Unified motion/force/impedance control for manipulators in unknown contact environments based on robust model-reaching approach," *IEEE/ASME Transactions on Mechatronics*, vol. 26, no. 4, pp. 1905–1913, 2021.

[19] N. Jiang, S. Zhang, J. Xu, and D. Zhang, "Model-free control of flexible manipulator based on intrinsic design," *IEEE/ASME Transactions on Mechatronics*, vol. 26, no. 5, pp. 2641–2652, 2020.

[20] X. Liu, S. S. Ge, F. Zhao, and X. Mei, "Optimized interaction control for robot manipulator interacting with flexible environment," *IEEE/ASME Transactions on Mechatronics*, vol. 26, no. 6, pp. 2888–2898, 2020.

[21] E. Pereira, S. S. Aphale, V. Feliu, and S. R. Moheimani, "Integral resonant control for vibration damping and precise tip-positioning of a single-link flexible manipulator," *IEEE/ASME Transactions on Mechatronics*, vol. 16, no. 2, pp. 232–240, 2010.

[22] Q. Meng, M. Zhu, X. Lai, Y. Wang, and M. Wu, "Iterative-learning-based motion planning and position control of a single-link flexible manipulator with vibration sensor hysteresis," *IEEE/ASME Transactions on Mechatronics*, vol. 29, no. 6, pp. 4560–4571, 2024.

[23] S. C. P. Gomes, V. S. da Rosa, and B. C. Albertini, "Active control to flexible manipulators," *IEEE/ASME Transactions on Mechatronics*, vol. 11, no. 1, pp. 75–83, 2006.

[24] A. Abe, "Trajectory planning for residual vibration suppression of a two-link rigid-flexible manipulator considering large deformation," *Mechanism and Machine Theory*, vol. 44, no. 9, pp. 1627–1639, 2009.

[25] L. Cui, H. Wang, and W. Chen, "Trajectory planning of a spatial flexible manipulator for vibration suppression," *Robotics and Autonomous Systems*, vol. 123, p. 103316, 2020.

[26] J. Qiao, H. Wu, and X. Yu, "High-precision attitude tracking control of space manipulator system under multiple disturbances," *IEEE Transactions on Systems, Man, and Cybernetics: Systems*, vol. 51, no. 7, pp. 4274–4284, 2019.

[27] S. A. A. Moosavian and R. Rastegari, "Disturbance rejection analysis of multiple impedance control for space free-flying robots," in *IEEE/RSJ International Conference on Intelligent Robots and Systems*, vol. 3. IEEE, 2002, pp. 2250–2255.

[28] H. Wu, J. Qiao, Y. Chen, and Z. Li, "Robust anti-disturbance coordination control for space manipulator systems with multiple disturbances," in *2018 37th Chinese Control Conference (CCC)*. IEEE, 2018, pp. 2601–2606.

[29] D. Meng, W. Lu, W. Xu, Y. She, X. Wang, B. Liang, and B. Yuan, "Vibration suppression control of free-floating space robots with flexible appendages for autonomous target capturing," *Acta Astronautica*, vol. 151, pp. 904–918, 2018.

[30] W. J. Marais, S. B. Williams, and O. Pizarro, "Anisotropic disturbance rejection for kinematically redundant systems with applications on an uvms," *IEEE Robotics and Automation Letters*, vol. 6, no. 4, pp. 7017–7024, 2021.

[31] Y. Maezawa, Y. Ambe, Y. Yamauchi, M. Konyo, K. Tadakuma, and S. Tadokoro, "Translational disturbance rejection for jet-actuated flying continuum robots on mobile bases," *IEEE Robotics and Automation Letters*, vol. 8, no. 11, pp. 7456–7463, 2023.

[32] F. L. Lewis, D. Vrabie, and V. L. Syrmos, *Optimal control*. John Wiley & Sons, 2012.

[33] J. M. Maciejowski, *Predictive Control with Constraints*. Pearson Education, 2002.

[34] S. Skogestad and I. Postlethwaite, *Multivariable feedback control: analysis and design*. john Wiley & sons, 2005.

[35] J. Han, "From PID to active disturbance rejection control," *IEEE Transactions on Industrial Electronics*, vol. 56, no. 3, pp. 900–906, 2009.

[36] Doosan-Robotics, "M1013," https://www.doosanrobotics.com/en/products/series/m1013, [Online] Accessed on 2024-09-30.

[37] D. J. Ewins, *Modal testing: theory, practice and application*. John Wiley & Sons, 2009.

[38] A. S. Chen, E. J. L. Pulgarin, G. Herrmann, A. Lanzon, J. Carrasco, B. Lennox, B. Carrera-Knowles, J. Brotherhood, T. Sakaue, and K. Zhang, "Dynamics-based trajectory planning for vibration suppression of a flexible long-reach robotic manipulator system," in *2024 IEEE/RSJ International Conference on Intelligent Robots and Systems (IROS)*. IEEE, 2024, pp. 8690–8695.

[39] W. Yang, G. Herrmann, X. Chen, and M. Lowenberg, "Dynamic gain scheduled control of a satellite with a robot manipulator," in *2010 3rd International Symposium on Systems and Control in Aeronautics and Astronautics*. IEEE, 2010, pp. 1151–1156.

[40] B. M. Chen, *Robust and H_∞ Control*. Springer Science & Business Media, 2013.

Anthony Siming Chen (Member, IEEE) obtained his M.Sc. and Ph.D. degrees in (Advanced) Mechanical Engineering with the Dynamics and Control Group from the University of Bristol in 2017 and 2022. He is now an Assistant Professor with the Department of Electrical and Electronic Engineering at the University of Nottingham, affiliated with the Mechanical and Aerospace Systems Research Group (MAS) and the Institute for Aerospace Technology (IAT). He also holds an honorary position with the Control Systems and Robotics Group (CSR) at the University of Manchester.

Dr. Chen is a RAICo Fellow, MIEEE, MIET, and Member of the Royal Aeronautical Society (MRAeS). His research sits at the intersection of control theory, machine learning, and robotics, with a particular focus on embodied intelligence and learning-based methods for complex real-world systems.

Erwin Jose Lopez Pulgarin (Member, IEEE) received the B.S. degree in Mechatronics Engineering from the Universidad Nacional de Colombia, Bogota, Colombia, in 2012 and his Ph.D. degree in Mechanical Engineering from University of Bristol, Bristol, UK, in 2019.

He is currently a Postgraduate Research Associate at The University of Manchester, working on robotics and HRI for challenging environments. His current research interests include human robot interaction, data-driven modelling, teleoperation and autonomous systems.

Guido Herrmann (Senior Member, IEEE) received the degree "Diplom-Ingenieur der Elektrotechnik" from the Technische Universität zu Berlin, Berlin, Germany, in 1997 and the Ph.D. degree in control from the University of Leicester, U.K., in 2001. Since 2019, he has been a Professor in Robotics and Intelligent Control at the University of Manchester, where he also leads the Control Systems and Robotics Group. He is an Honorary Professor at the University of Bristol.

Prof. Herrmann is a Fellow of the IET and has been awarded with Dr. Jing Na the 2017 Hsue-shen Tsien Paper Award. His research interests include the development and application of novel, robust and nonlinear controllers with high-impact applications in robotics, automotive and high-precision systems.

Alexander Lanzon (Senior Member, IEEE) received his Ph.D. degree in Control Engineering and his M.Phil. degree in Robot Control from the University of Cambridge, UK, in 2000 and 1997, and received his B.Eng.(Hons). degree in Electrical and Electronic Engineering from the University of Malta, Malta, in 1995. In 2006, he joined the University of Manchester, UK, where he now holds the Chair in Control Engineering.

Prof. Lanzon is a Fellow of the Institute of Mathematics and its Applications, the Institute of Measurement and Control, and the Institution of Engineering and Technology. He held editorial roles with IEEE Control Systems Letters (2023-2024), IEEE Transactions on Automatic Control (2013-2019), and the International Journal of Robust and Nonlinear Control (2012-2015). His research interests include the fundamentals of feedback control theory, negative imaginary systems theory, robust control, nonlinear control, and their applications to robotic motion control problems.

Joaquin Carrasco (Member, IEEE) is a Reader in the Control Systems and Robotics Group, Department of Electrical and Electronic Engineering, University of Manchester, UK. He was born in Abaran, Spain, in 1978. He received the B.Sc. degree in Physics and the Ph.D. degree in Control Engineering from the University of Murcia, Murcia, Spain, in 2004 and 2009, respectively. From 2009 to 2010, he was with the Institute of Measurement and Automatic Control, Leibniz University Hannover, Germany. From 2010 to 2011, he was a research associate and, since 2011, he is an academic at the School of Engineering, University of Manchester, UK. His current research interests include absolute stability, learning in control, and robotics applications.

Barry Lennox (Senior Member, IEEE) Barry Lennox is Fellow of the Royal Academy of Engineering and Professor of Applied Control and Nuclear Engineering Decommissioning at The University of Manchester. He holds a Royal Academy Chair in Emerging Technologies and was the Director of the Robotics and Artificial Intelligence for Nuclear (RAIN) Research Hub that received £15M of funding through the ISCF Robotics for a Safer World programme.

Professor Lennox is also the academic lead for the Robotics and Artificial Intelligence Collaboration (RAICo) programme, which aims to deliver robotic technology to support the decommissioning of fission and fusion facilities in the UK and is the Academic Director of the CRADLE Prosperity Partnership between Amentum and The University of Manchester.

John Brotherhood is a Senior Principal Robotics Specialist at Amentum (formerly Jacobs) working as a subject matter expert in robotics and remote handing in complex environments focusing on removing humans from harm.

He is a degree qualified engineer with over 20 years' experience spanning the full design lifecycle from conceptual design studies, research and development, management of test and performance trials through to successful implementation.

Tomoki Sakaue (Member, IEEE) received his M.Eng. degree in Electrical and Electronic Engineering from Tokyo Institute of Technology, Japan, in 1999. He has been working as a senior researcher in robotics at Tokyo Electric Power Company (TEPCO) Holdings.

Mr. Sakaue was elected the Finalist for Best Paper at the 15th IEEE International Symposium on Safety, Security and Rescue Robotics in 2017 for his work on deployment of decommissioning robot.

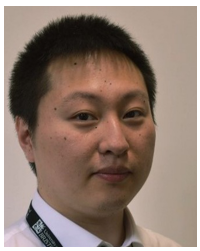

Kaiqiang Zhang (Member, IEEE) received his B.Eng. degree in Automatic Control from the Xi'an Jiaotong University in 2012, his M.Sc. (dist.) degree in Advanced Engineering Robotics and Ph.D. degree in Control from the University of Bristol, in 2013 and 2019, respectively.

He is a Principal Researcher in Deployment Systems, Payloads Handling, and Maintenance Automation at the United Kingdom Atomic Energy Authority, where he is the Programme Area Manager of Robotics Research at UKAEA. His research interests include robust control, adaptive control, nonlinear modelling, motion planning algorithms and the associated robotic applications.